Nuclear Inst. and Methods in Physics Research, A 871 (2017) 72–76

Contents lists available at ScienceDirect

Nuclear Inst. and Methods in Physics Research, A

journal homepage: www.elsevier.com/locate/nima

New tools for grazing incidence neutron scattering experiments open perspectives to study nano-scale tribology mechanisms

H. Frielinghaus [a,*], M. Gvaramia [a], G. Mangiapia [a], S. Jaksch [a], M. Ganeva [a], A. Koutsioubas [a], S. Mattauch [a], M. Ohl [b], M. Monkenbusch [b], O. Holderer [a]

[a] Jülich Centre for Neutron Sciences at MLZ, Forschungszentrum Jülich GmbH, Lichtenbergstrasse 1, 85747 Garching, Germany
[b] Jülich Centre for Neutron Sciences JCNS-1, Forschungszentrum Jülich GmbH, Leo Brandt Straße, 52425 Jülich, Germany

ARTICLE INFO

Keywords:
Tribology
Neutron spectroscopy
Surface dynamics
Grazing incidence scattering
Enhanced waves

ABSTRACT

Using grazing incidence scattering methods allows for depth profiling near surface structures very efficiently Dosch (1986). In parallel, layered structures have been used as resonators to enhance the wave field Kozhevnikov et al. (2007), Khaydukov et al. (2011), Kozhevnikov et al. (2011) and Nesnidal and Walker (1996) that directly increases the scattered intensity too. Third, the combination of these methods with neutron spin echo spectroscopy allows for near surface studies of dynamics Jaksch et al. (2015) and Frielinghaus et al. (2012) that can be correlated to tribological effects on the molecular level. This field of science, the tribology, – so far – has been driven mainly by the surface force balance that measures the macroscopic response of the system (latest research employs also AFM) Raviv et al. (2003) [1], Chung et al. (2016) [2] and Mocny and Klok (2016) [3]. The progress of this method was to reach the nano-scale distances that were necessary to obtain information about the friction of the nano-structures. The proposed method of grazing incidence neutron spin echo spectroscopy gives access to much more detailed information of molecular response to confinement by one or two hard walls, and therefore would pave the way for very rich and precise tribological comparisons of theory with experiments.

1. Introduction

Complex fluids display a rich behavior at their interfaces to other materials that has been studied experimentally [4–12] and theoretically [13–15]. Practically, one often conducts reflectometry or grazing incidence small angle scattering experiments to obtain the structure in the normal and lateral dimensions. Close to the interface one finds an interphase of modified structure [4] compared to the bulk phase depending on the system. So for instance there can be oriented liquid crystalline order in the interphase while the bulk shows only short-range order without orientation [16] The evanescent wave in a GISANS experiment is used to highlight a certain region of depth Λ next to the interface. Varying this scattering depth Λ, allows for depth profiling in much more detail compared to simple reflectometry experiments. At this stage, the near-surface structure might support specific contact-sensitive applications of complex fluids.

The idea of highlighting different regions next to the interface was then transferred to neutron spin echo spectroscopy [17], where the dynamics of microemulsions was analyzed as a function of depth Λ. Practically, the dynamics were three times faster than the bulk, which was explained by the confinement of the lamellar membranes adjacent to the interface. The volume conservation leads to a faster feedback of the neighboring membranes and/or the solid interface. This finding, then, was connected to the lubrication effect, which means that parallel lamellae can slide off along the interface faster than the disoriented bulk structure. From this example the general topic of tribology was raised. GINSE measurements will open a new research area on friction effects that now can be analyzed on the nano-scale [18].

At this point the field of tribology that has been mainly driven by the surface force balance that measures the macroscopic response of the system [1–3] will get deeper insight from a new method.

The instrumental elements that were developed to accompany the new findings in GINSE experiments are discussed in this manuscript. On the one hand, neutron experiments need to relax the resolution in order to observe reasonable intensities on the detector. This is especially prominent for NSE experiments, because the method requires very high statistics with spin polarization analysis [17]. On the other hand, grazing incidence scattering experiments require the slit geometry

* Corresponding author.
E-mail address: h.frielinghaus@fz-juelich.de (H. Frielinghaus).

http://dx.doi.org/10.1016/j.nima.2017.07.064
Received 3 May 2017; Received in revised form 24 July 2017; Accepted 31 July 2017
Available online 5 August 2017

at the entrance aperture and for the sample to define the incident angle (and the scattering depth Λ), which reduces the number of neutrons dramatically On top, the evanescent wave is only seen by the near surface structure within a distance of 40 to 100 nm, which heavily restricts the scattering volume. The first experiments sufficiently overcame the problem by huge interfaces and by samples that scatter intrinsically strong. The boundary condition at total reflection used in the grazing incidence method yields a factor of 2 for the immediate amplitude of the evanescent wave at the interface which results in an intensity gain of 4 compared to a plain illumination of the boundary layer.

Neutron waveguides have been developed to increase the scattering intensities from a highlighted zone even further [18]. In principle, two situations must be distinguished: The structure of interest lies within or outside the waveguide. The first situation limits the use of the waveguide to one specific application, while a separate waveguide with the intensity enhancement outside would be of wider interest for a whole set of samples, because the complex fluid next to the waveguide can be replaced easily. The manuscript summarizes the recent developments and highlights the waveguide as the missing part for studying tribology effects of complex fluids in contact with solids.

2. Instruments

Neutron reflectivity measurements have been performed at **MARIA** at FRM2 in Garching [19]. This instrument uses neutron velocity selector with a 10% bandwidth for highest intensities. We used wavelengths of 10 and 5 Å for higher (incident angle $\alpha_i < 1.5°$) and lower ($\alpha_i > 1°$) resolution. The vertical entrance and sample slits were of 2 mm × 5 cm size (1.5 cm at sample). The samples were kept in closed cells with a sample thickness of 0.5 mm, but large areas of ca. 13 × 5 cm at a silicon slab of 15 × 8 × 4 cm^3. The neutrons impinge through the silicon, get reflected at the solid/liquid interface and leave through the silicon. The whole cell is heated to 26 °C through a water mediated heater. The sample is aligned and positioned by a hexapod. More details of the instrument can be found in Ref. [19].

Neutron spin echo spectroscopy experiments have been performed at the **J-NSE**, Garching and the **SNS-NSE**, Oak Ridge. The first instrument used a single wavelength of 8 Å (10% velocity selector) while the second one used a wavelength band of 5 to 8 Å. The latter analyzed the actual wavelength by time of flight analysis to a resolution of ca. ±0.1 Å. Both instruments were equipped with an additional entrance aperture of 2 mm x 6 cm. Close to the sample cell (as described above) unwanted neutron paths were blocked using boron and cadmium based materials. Acquisition times for one scattering vector and the full range of Fourier times were ca. 1 day. Further details of the instruments are found in Refs. [20,21] and [22].

3. GINSES measurements

Two example measurements of relaxation curves for the systems SoyPC in D_2O [18] and a bicontinuous microemulsion, both adjacent to a hydrophilic silicon surface, are shown in Fig. 1. We used the two proposed tools, i.e. a neutron prism and the resonator simultaneously for this measurement. The lipid L-alpha-phosphatidylcholine from soybeans (SoyPC) forms well ordered lamellar bilayers close to the solid–liquid interface [23]. While the Bragg peak of this structure is well pronounced and quite sharp, the bilayer relaxations are observed much better at scattering vectors deviating from the Bragg peak, which virtually shows no dynamics (DeGennes narrowing). This implies the use of Q-values with low intensities, where, however, a reasonable fluctuation dynamics signal dominates the scattering and grazing incidence neutron spin echo experiments can be performed. Thus, the resonator was extremely important to obtain meaningful statistics. Interestingly, the asymmetry of incident and exit angles lead to a rather small in-plane scattering vector that made collective long-wavelength modes visible,

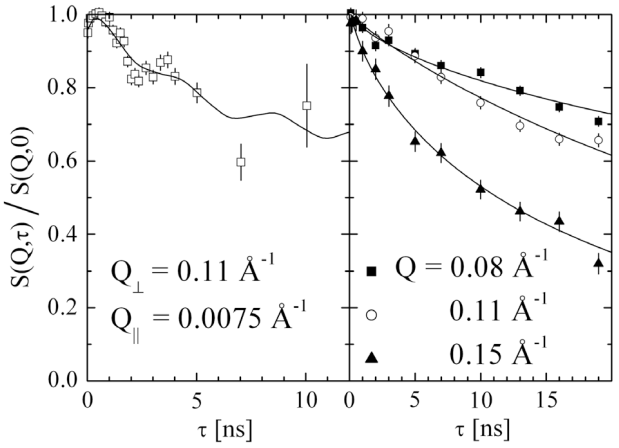

Fig. 1. The relaxation curves measured by grazing incidence neutron spin echo spectroscopy of lamellar lipid bilayer stacks (left) and of a bicontinuous microemulsion with lamellar near-surface ordering (right). The scattering depth was 200 and 240 Å. While the incidence angles were below the critical angle of total reflection, the exit angles were at considerable values according to the indicated Q (or $Q_\perp$). This asymmetry lead to in-plane $Q_\parallel$ vectors that are essential for the physics of well oriented lipid bilayers (left) but negligible in the case of microemulsions (right, where omitted).

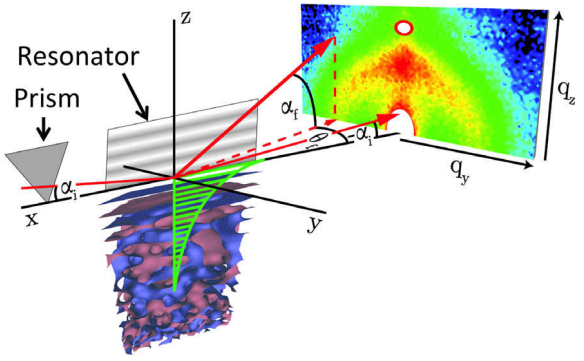

Fig. 2. The scattering geometry of a grazing incidence neutron spin echo spectroscopy (GINSES) experiment using a neutron prism and a resonator that is ideally suited for pulsed neutron sources. The sample is a microemulsion adjacent to the layered resonator structure. The green area inside the microemulsion indicates the enhanced evanescent wave. The detector plain shows a typical scattering image of a microemulsion. The red open dot indicates the typical Q-vector of the GINSES experiment.

that possessed enough elasticity to overcome the usual over-damping of soft matter systems. These modes allow for energy dissipation over large distances, and might explain the stability of cartilage in joints. The cartilage consists of proteins and lamellar lipid arrangements [24,25].

The set of the prism and resonator also allowed the strongly scattering microemulsion to be characterized at higher scattering angles, where the intensities decrease considerably (Sketch in Fig. 2). While first measurements without resonator were successfully analyzed at intermediate scattering vectors, where the collective and single-membrane modes still mix, the experiments presented here allow for analyzing smaller length scales where only single-membrane modes meet the theoretically well developed model of Zilman and Granek. The confinement conditions by the solid surface lead to an extension by the theory of Seifert [17]. The intensity gain of the microemulsion through the resonator was ca. 3.

The asymmetric setting of the GINSES experiment (Fig. 2) goes back on the condition of the incident angle α_i, which must be below the critical angle of total reflection α_c. So the exit angle α_f is much bigger than α_i. This causes a small in plane Q-vector component $Q_\parallel$ that is essential for the observation of the viscoelastic behavior of lipid bilayer stacks, but negligible for microemulsions. The normal component $Q_\perp$ is always dominating.

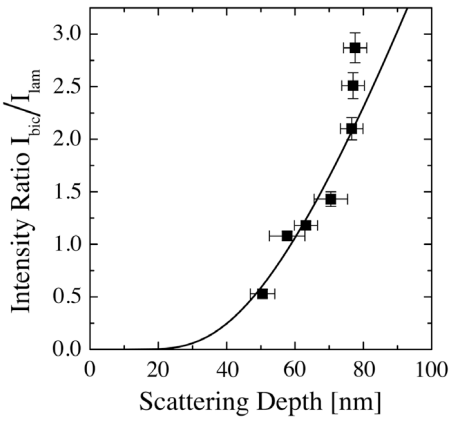

Fig. 3. The GISANS intensity ratio of a bicontinuous microemulsion with lamellar order adjacent to the solid–liquid interface [16]. The solid line corresponds to the theoretical ratio of the Laplace transformations of the bicontinuous and lamellar zones $I_{bic}/I_{lam} = I_{bulk}/I_{interphase}$.

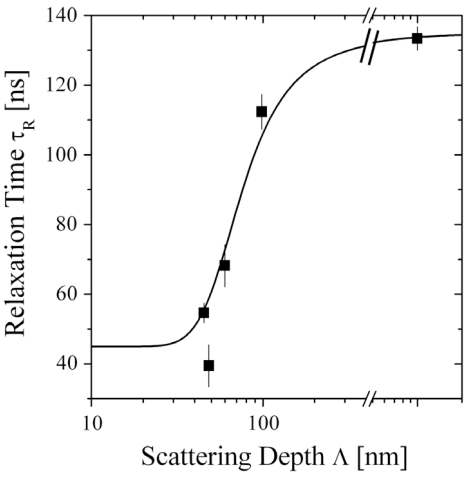

Fig. 4. The relaxation time of the microemulsion dynamics at different scattering depths Λ [17]. The interpolation curve is obtained from the intensity ratio of the static scattering (Fig. 3). The rightmost tick indicates the bulk sample (of virtually infinite thickness compared to the nano-scale).

4. The depth resolution

The scattered intensity of an evanescent wave in the (fluid) sample can be described by a simple matrix element that arises from the (distorted wave) Born approximation [35] according to:

$$I \propto \left|\langle \exp(-i\vec{k}_f\vec{r})|\rho(\vec{r})|\exp(i\vec{k}_i\vec{r}_{xy} - z/\Lambda)\rangle\right|^2.$$

Here we separate the real and imaginary part of the incidence wave vector, while we assume that the wave vector $\vec{k}_f$ of the final (scattered) wave is real, i.e. the exiting wave is not tunneling. The scattering depth for neutron scattering experiments is given by [16]:

$$\Lambda = \left[4\pi \cdot \Delta\rho \cdot (1 - \alpha_{in}^2/\alpha_c^2)\right]^{-1/2}.$$

Here, $\Delta\rho$ is the scattering length density difference between the sample and the other hemisphere, and the critical angle of total reflection is $\alpha_c = \lambda\sqrt{\Delta\rho/\pi}$, with λ being the neutron wavelength. This concept for the scattering depth holds for negligible absorption (that most materials have) and for exiting waves at rather large angles (considerably larger than α_c).

If the sample has small correlation volumes (smaller than Λ), the sub-volumes scatter independently, and the collected scattering signal from an interphase and the bulk corresponds to a Laplace-transformation of the two zones [26]. One obtains:

$$I_{interphase} \propto \xi^3(1 - \exp(-2Z/\Lambda))$$
$$I_{bulk} \propto \xi^3 \exp(-2Z/\Lambda).$$

The correlation volume ξ^3 is connected to the correlation length ξ. The argument of the exponential is doubled, because the modulus of the matrix element is squared. The often discussed intensity ratio from bulk versus interphase characteristics displays a linear asymptote with an extrapolated intercept that exactly agrees with the interphase thickness Z This strong simplification might lead to slightly wrong (10%–20%) results, and mainly has to be seen as a first guess tool.

Experimental data points for the abovementioned intensity ratio are depicted in Fig. 3. The bulk scattering results from an isotropic Debye–Scherrer ring from the bicontinuous microemulsion, and the lamellar interphase is represented by a Bragg peak that indicates similar repeat distances compared to the bulk. The linear extrapolation to the virtual zero intensity determines the interphase thickness of ca. 40 nm, while the suggested Laplace transformation would lead to a lamellar interphase thickness of ca. 85 nm

The second experimental result is the relaxation times measured by GINSES of the same microemulsion at different scattering depths (Fig. 4). The intensity ratio from the structural analysis (Fig. 3) gives rise to the interpolation curve that interpolates between the interphase and the bulk relaxation times of 45 and 135 ns. Thus, the structural interpretation agrees between the static and dynamic scattering.

4.1. The first tool: the neutron prism

A neutron prism used for grazing incidence scattering experiments allows for correcting the incidence angle as a function of wavelength according to the critical angle of total reflection [27], which is extremely important for pulsed neutron sources with broad wavelength bands in use. The latter is a linear function of the neutron wavelength according to $\alpha_c = \lambda\sqrt{\Delta\rho/\pi}$, while the incidence angle correction δ_{exit} is a quadratic function of the wavelength according to:

$$\delta_{exit} = \delta_0 - \frac{\rho}{\pi} \cdot \frac{\lambda^2}{\varepsilon}.$$

Here δ is the incident angle of a beam with respect to the base of the prism, which basically is not corrected. The sharp angle ε at the base of the prism must fulfill the condition $1 \gg \varepsilon \gg \delta_0, \delta_{exit}$ (all angles in radian). The obtuse tip of the prism is pointing down in this notation. The correction of the incident angle with respect to the critical angle is possible, because the considered wavelength band is distributed around finite wavelengths where a parabolic dependence can be considered to be locally linear. The range of scattering depths is considerably narrowed by the correction. This correction was used at the spallation source SNS in Oak Ridge for grazing incidence neutron spin echo experiments on microemulsions at a hydrophilic silicon surface. There the wavelength band spanned the range from 5 to 8 Å. Alternatively the prism can also be used for classical instruments at reactors, where the typical wavelength distribution is ±5% or ±10%. Then, angles very close to the critical angle α_c can be accessed with the wings of the wavelength distribution not leading to neutrons that penetrate the sample deeply. This would also lead to sharper reflectivity curves of selector-based reflectometers.

4.2. The essential tool: a neutron resonator

Layered structures to obtain constructive interference have been considered already for neutrons with the sample of interest being within the layered structure [28–30], and for light waves with the sample being outside [31]. The development of the neutron resonator described below aims at the enhanced scattering from samples being adjacent (but outside) to the resonator, and is apparently presented for the

first time. Because the physics of the resonator and of the reflectivity scale simultaneously with the used wavelength, the representation of all results in Q-space would be natural. Additionally, the incidence angle correction by the prism leads to a rather well irradiated resonance for all wavelengths that is furthermore supported to a larger entrance aperture towards zero incidence angles. The resonator will work properly as long as the critical Q_c of total reflection is bigger than the Q-values of the resonance(s), i.e. $Q_c = 4\pi(\Delta\rho/\pi)^{1/2} > Q_{\mathrm{reso}} \approx 0.011$ Å$^{-1} \approx Q_{001} = 2\pi/d$ (with d being the repeat distance of the layered structure). The separation of the layered structure from the sample makes the usage of the resonator more universal, and allows for reusing the costly parts.

The base material that covers the upper hemisphere is still silicon, due to its purity, its ability for layers being sputtered on top easily, and for its scattering length density (2.07×10^{-6} Å^{-1}) being in a reasonable range between fully hydrogenous (ca. -0.6×10^{-6} Å^{1}) and deuterated (ca. 6–7$\times$ 10^{-6} Å^{-1}) soft matter samples. Apart from that, rather large silicon slabs can be obtained at relatively low cost that allow for large interfaces and large scattering angles. Especially for grazing incidence neutron scattering experiments, the large sample is important because even the most powerful neutron sources are left behind the modern synchrotrons. This is also why the development of the neutron resonator with gain factors of about 10 is highly important.

The studied double layers consist of titanium and platinum while at all multiples of double layers there is one finishing layer of titanium. These two materials are ideally suited for the sputtering, and serve for rather low and high scattering length densities (i.e. −1.91 and 6.36$\times$ 10^{-6} Å^{-1}) even at natural isotope abundances.

The first resonator that we produced had three double layers with a single finishing titanium layer. From simulations with the BornAgain package [32] we can see the mechanism of the resonator (see Fig. 5). The critical angle of total reflection is at around 0.5° (where the neutrons fully penetrate into the heavy water), still representing the scattering length density difference between silicon and heavy water. The repeat distance of the double layers is placed at scattering angles below the critical angle (i.e. $Q_{001} < Q_c$ representing the first order Bragg and the critical scattering angle with $Q_x = 4\pi \sin(\alpha_x)/\lambda$ and $Q_{001} = 2\pi/d$ with $d = (130 + 320)$ Å), such that here the resonances are observed. Interestingly, three distinguished resonances appear corresponding to one, two and three maxima in the waveguide. The corresponding evanescent wave is strongly enhanced in the heavy water. The original idea of this resonator was that three different incident angles could be chosen for still different scattering depths. However, for the first GINSE experiments all three resonances were irradiated for highest intensities, neglecting the possibility of different better defined scattering depths. Accidentally, the number of complete double layers corresponds to the number of resonances, while the elementary magnitude is the overall thickness of the whole resonator structure that can host the according number of resonances. Apart from that, it became obvious that the sharp resonances collimate the incident beam further. When we discuss gain factors, we refer to usual collimations of ca. 0.03° without resonator such that the maximal possible gains lie in the range of 10. We are aware that within the resonance amplifications can be 100 and 1000 or more, but they do not directly translate to realistic gain factors since they apply for very narrow divergence bands of incoming neutrons covering only a small subband of the actually used illumination

From this result, we simulated the off-specular scattering in a reflectometry experiment, where the incident and exit angles (α_i and α_f) are varied (Fig. 6). Along the specular reflectivity line the 2nd order Bragg peak appears around 0.9° while the critical angle is around 0.7°. The intensities in between drop stronger in the simulations compared to the experiment which might be an issue of resolution. The structures in the perpendicular direction arise from surface roughness, and are nearly invisible One observes further expressions of the resonances at either small incident or at small exit angles (α_i or $\alpha_f < \alpha_c$). The two characteristic sinusoidal lines in the horizontal and vertical direction are another expression of the roughness: While the periodicity is connected

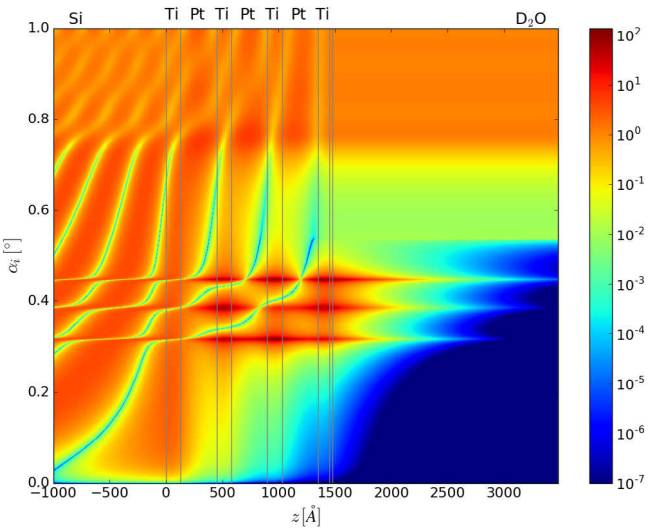

Fig. 5. Intensity distributions in the resonator for different incident angles α_i at different depths z inside the structure ($\lambda = 8$ Å). There are the following materials involved: silicon ($z < 0$), four titanium layers of 130 Å thickness (for the top one we assumed an oxidization layer of 30 Å), three platinum layers of 320 Å, and heavy water ($z < 1480$ Å). The critical angle of total reflection lies at around 0.5°, where the neutrons fully penetrate the heavy water. Three resonances are observed with differing numbers of maxima in the waveguide (1, 2, and 3).

to the double layer periodicity of the resonator structure, the intensity decay with increasing angles is connected to the in-plane correlation length ξ. Experimentally, these features are a little stronger which might be connected to a larger ξ.

The experimental and theoretical specular reflectivities are compared for the resonator against plain heavy water and the soyPC lipid bilayer stacks in heavy water (Fig. 7). The important second order Bragg peak is observed for an incident angle larger than the critical angle of total reflection. Higher order fringes are partially covered by the measurements, but much weaker than the simulations would predict. This is due to imperfections (roughness and material diffusion) of the resonator structure on small length scales and instrumental resolution. For the resonator against the soyPC stacks, the SoyPC scattering adds up incoherently on top of the resonator structure due to the separation of length scales (i.e. 450 Å vs. 60 Å). The lipid bilayer stack was modeled by 76 and 20 bilayers on top of each other with a repeat distance of 56 and 62 Å, respectively. This modeled the broad Bragg peaks of the lipid structure reasonably well, although we see that the measurement is affected by finite resolution due to the wavelength spread (FWHM 10%) and soft matter structures usually appear with broader peaks. Apart from the imperfections of the resolution/size distribution effects, incoherent and instrumental background becomes an issue at reflectivities around 10^{-5} and below.

Very important is the intensity dip within the plateau of total reflection [29]. Here, neutrons are scattered from the enhanced wavefield by the sample that are then finally missing in the specular reflex. This is a proof for the resonator working properly. This kinematic effect is not simulated by the distorted wave Born approximation that only covers kinematic effects for the specular reflectivity, i.e. the wave distortions in the normal direction.

The understanding of resonances dates back to mechanical systems over laser resonators and nuclear scattering effects to the actual multilayers for enhanced scattering intensities. All of them have in common, that the energy of impinging fields is collected to yield a higher energy density in the resonator. This does not contradict the Liouville theorem, because the density of phase space is not directly correlated with the density of energy.

The obtained gain factors of ca. 3 in the GINSE experiments (NSE count rates for microemulsions at reactor sources grow from ca. 20

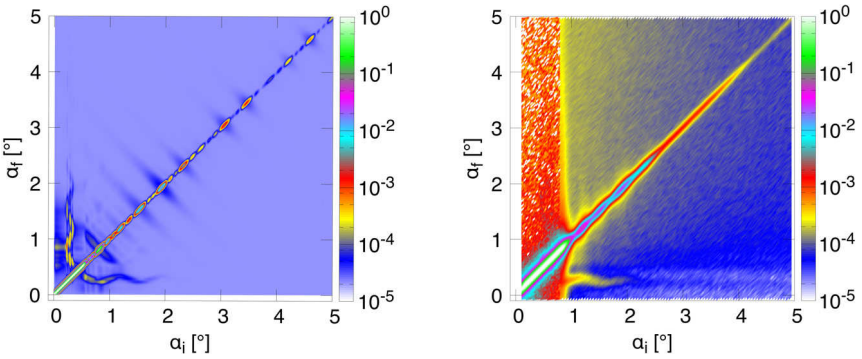

Fig. 6. Simulated and experimental off-specular scattering of the resonator with surface roughness (rms = 0.1 nm, correlation length ξ = 1 μm, and the hurst parameter = 0.8 [33,34], λ = 6 Å, constant background added to theory).

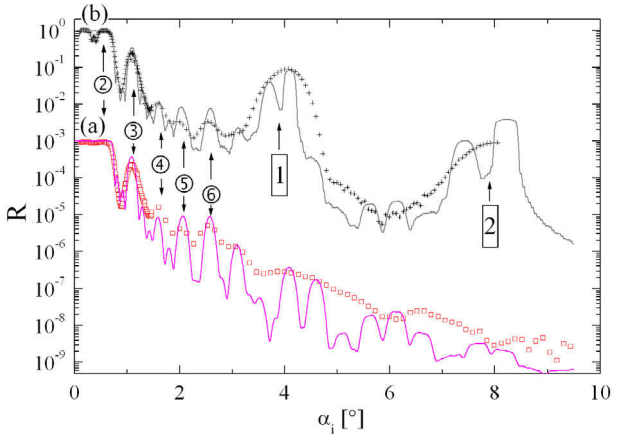

Fig. 7. (a): Reflectivity of the resonator against plain heavy water (λ = 8 Å) scaled by 10^3 (open boxes, with errors within the symbol size). One observes the second order Bragg peak of the wave guide structure at around α_i = 1°(⬢) Higher order fringes (⬢...⬢) of the simulations (solid line) are partially expressed by the measurements. (b): Reflectivity of the resonator against the lamellar soyPC lipid bilayer stack (crosses). The additional important first order Bragg peak at α_i = 4° (1) arises from the lipid bilayers (the second order (2) is partially covered by the measurements).

to 60 and 100 counts per second) are lower than the maximal gains of 10 from the simulations. Current developments are ongoing with reduced waviness of the silicon wafers, because we assume that correlations at 1 to 10 μm distances are important for the constructive interference. Thus, we are optimistic to present the experimental proof for the maximal gain of ca. 10 in the near future. By this the way will be paved for extensive studies of tribological effects on the molecular level using grazing incidence neutron spin echo spectroscopy.

References

[1] U. Raviv, S. Giasson, N. Kampf, J.-F. Gohy, R. Jérôme, J. Klein, Nature 425 (2003) 163–165.
[2] P.S. Chung, M.S. Jhon, H.J. Choi, Soft Matter 12 (2016) 2816–2825.
[3] P. Mocny, H.-A. Klok, Mol. Syst. Des. Eng. 1 (2016) 141–154.
[4] P. Lang, J. Phys.: Condens. Matter. 16 (2004) R699–R720.
[5] P. Lang, L. Willner, W. Pyckhout-Hintzen, R. Krastev, Langmuir 19 (2003) 7597–7603.
[6] F. Cousin, J. Jestin, G. Chaboussant, S. Gautrot, A. Menelle, F. Ott, Eur. Phys. J 167 (2009) 177–183.
[7] R. Steitz, P. Müller-Buschbaum, S. Schemmel, R. Cubitt, G. Findenegg, Europhys. Lett. 67 (2004) 962–968.
[8] M. Wolff, U. Scholz, R. Hock, A. Magerl, V. Leiner, H. Zabel, Phys. Rev. Lett. 92 (2004) 255501.
[9] W. Hamilton, L. Porcar, L. Magid, Physica B 357 (2005) 88–93.
[10] G. Salamat, R. de Vries, E. Kaler, S. Satija, L. Sung, Langmuir 16 (2000) 102–107.
[11] G. Brotons, L. Belloni, T. Zemb, T. Salditt, Europhys. Lett. 75 (2006) 992–998.
[12] A. Vorobiev, G. Gordeev, O. Konovalov, D. Orlova, Phys. Rev. E 79 (2009) 031403.
[13] F. Schmid, J. Phys.: Condens. Matter 10 (1998) 8105–8138.
[14] M. Müller, K. Binder, Phys. Rev. E 63 (2001) 021602.
[15] B. Cichocki, E. Wajnryb, J. Blawzdziewicz, J.K.G. Dhont, P. Lang, J. Chem. Phys. 132 (2010) 074704-1–074704-12, dynamics.
[16] M. Kerscher, P. Busch, S. Mattauch, H. Frielinghaus, D. Richter, M. Belushkin, G. Gompper, Phys. Rev. E 83 (2011) 030401(R).
[17] H. Frielinghaus, M. Kerscher, O. Holderer, M. Monkenbusch, D. Richter, Phys. Rev. E 85 (2012) 041408.
[18] S. Jaksch, O. Holderer, M. Gvaramia, M. Ohl, M. Monkenbusch, H. Frielinghaus, Sci. Rep. 7 (4417) (2017) 7.
[19] Heinz Maier-Leibnitz Zentrum, et al., MARIA: magnetic reffectometer with high incident angle, J. Large-Scale Res. Facil. 1 (2015) A8. http://dx.doi.org/10.17815/jlsrf-1-29.
[20] O. Holderer, M. Monkenbusch, R. Schätzler, H. Kleines, W. Westerhausen, D. Richter, Meas. Sci. Technol. 19 (2008) 034022, 6 pages.
[21] Heinz Maier-Leibnitz Zentrum, et al., J-NSE: neutron spin echo spectrometer, J. Large-Scale Res. Facil. 1 (2015) A11. http://dx.doi.org/10.17815/jlsrf-1-34.
[22] M. Ohl, M. Monkenbusch, N. Arend, T. Kozielewski, G. Vehres, C. Tiemann, M. Butzek, H. Soltner, U. Giesen, R. Achten, H. Stelzer, B. Lindenau, A. Budwig, H. Kleines, M. Drochner, P. Kaemmerling, M. Wagener, R. Möller, E.B. Iverson, M. Sharp, D. Richter, Nucl. Instrum. Methods Phys. Res. A 696 (2012) 85–99.
[23] S. Jaksch, F. Lipfert, A. Koutsioubas, S. Mattauch, O. Holderer, O. Ivanova, H. Frielinghaus, S. Hertrich, S.F. Fischer, B. Nickel, Phys. Rev. E 91 (2015) 022716.
[24] Mirea D.A., A.M. Trunfio-Sfarghiu, C.I. Matei, B. Munteanu, A. Piednoir, J.P. Rieu, M.G. Blanchin, Y. Berthier, Tribol. Int. 59 (2013) 302–311.
[25] Z. Pawlak, W. Urbaniak, M. Hagner-Derengowska, W. Hagner, Cell Biochem. Biophys. 71 (2015) 1615–1621.
[26] H. Dosch, B.W. Batterman, D.C. Wack, Phys. Rev. Lett. 56 (1986) 1144–1147.
[27] H. Frielinghaus, O. Holderer, F. Lipfert, M. Monkenbusch, N. Arend, D. Richter, Nucl. Instrum. Methods Phys. Res. A 686 (2012) 71–74.
[28] S.V. Kozhevnikov, F. Ott, E. Kentzinger, A. Paul, Physica B 397 (2007) 68–70.
[29] Y.N. Khaydukov, V.L. Aksenov, Y.V. Nikitenko, K.N. Zhernenkov, B. Nagy, A. Teichert, R. Steitz, A. Ruühm, L. Bottyán, J. Supercond. Nov. Magn. 24 (2011) 961–968.
[30] S.V. Kozhevnikov, A. Rühm, F. Ott, N.K. Pleshanov, J. Major, Physica B 406 (2011) 2463–2466.
[31] R.C. Nesnidal, T.G. Walker, Appl. Optics 35 (1996) 2226–2229.
[32] J. Burle, C. Durniak, J.M. Fisher, M. Ganeva, G. Pospelov, W. Van Herck, J. Wuttke, BornAgain — software for simulating and fitting X-ray and neutron small-angle scattering at grazing incidence, http://www.bornagainproject.org, Version 181, 2017.
[33] J.-P. Schlomka, M. Tolan, L. Schwalowsky, O.H. Seeck, J. Stettner, W. Press, Phys. Rev. B 51 (1995) 2311–2321.
[34] S.K. Sinha, E.B. Sirota, S. Garoff, H.B. Stanley, Phys. Rev. B 38 (1988) 2297–2311.
[35] V. Holy, T. Baumbach, Phys. Rev. B 49 (1994) 10668–10676.